

Mimicking dark matter in clusters through a non-minimal gravitational coupling with matter: the case of the Abell cluster A586

Orfeu Bertolami*

*Departamento de Física e Astronomia, Faculdade de Ciências, Universidade do Porto,
Rua do Campo Alegre 687, 4169-007 Porto, Portugal[†]*

Pedro Frazão[‡] and Jorge Páramos[§]

*Instituto de Plasmas e Fusão Nuclear,
Instituto Superior Técnico
Av. Rovisco Pais 1, 1049-001 Lisboa, Portugal
(Dated: June 15, 2022)*

In this work, one shows that a specific non-minimal coupling between the scalar curvature and matter can mimic the dark matter component of relaxed galaxy clusters. For this purpose, one assesses the Abell Cluster A586, a massive strong-lensing nearby relaxed cluster of galaxies in virial equilibrium, where direct mass estimates are possible. The total density, which generally follows a cusped profile and reveals a very small baryonic component, can be effectively described within this framework.

PACS numbers: 04.20.-q, 04.50.Kd, 04.40.Nr

I. INTRODUCTION

In the last two decades, cosmology has acquired a new standing due to a wide range of observations of high precision data [1, 2]. These observations seem to reveal that the two dominant components of the universe are a non-baryonic form of matter, the so-called dark matter [3], and an exotic form of energy, dark energy [4]. The former leads to structure formation and the last is responsible for the present accelerated expansion of the universe. The search for an explanation for the existence and properties of these dark components of the Universe has prompted a strong debate about their origin and nature.

The behaviour of the galaxy rotation curves and the mass difference in clusters of galaxies suggest the existence of a non-interacting form of matter, the so-called dark matter, at galactic and extra-galactic scales respectively. The presence of this sort of matter is revealed only through its gravitational interaction, since it presumably does not interact via any other detectable way. For instance, an evidence for the existence of dark matter is the velocity dispersion of clusters that, combined with its morphological features, leads one to conclude that the overall mass should be far greater than the visible mass.

Amongst modified gravity theories, those which introduce higher order curvature terms in the Einstein-Hilbert action — and in particular the $f(R)$ theories of gravity [5, 6] — offer alternative explanations for these problems, along with other strong motivations coming from cosmology, astrophysics and high-energy physics [7].

Recently it was shown that, in the context of power-law theories, $f(R) \sim R^n$, the rotation curves can be explained as a curvature effect [8, 9]; a similar result [10] is also obtained in another extension of gravity that relies not only on a non-trivial curvature term, but also on a non-minimal coupling between matter and geometry [11].

Clusters are the largest structures whose masses can be measured in a reliable form, since they constitute the largest configuration of objects that passed through gravitational relaxation and entered into virial equilibrium [12]. The measuring methods, X-rays and gravitational lensing for visible and dark matter respectively, reveal that the masses of clusters are approximately seven to ten times larger than the total combined mass of stars and hot gas in the intracluster medium (ICM). This missing mass is predominant in the inner regions of clusters, but it is also extended beyond the core radius, as defined by the gas density distribution.

In the context of modified Newtonian Dynamics (MOND) [13], another popular (albeit incomplete [14]) alternative to General Relativity (GR), it is difficult to explain cluster observations without the assumption of “real” dark matter, because the mass of the dark component is otherwise significantly reduced but not completely removed [15].

The problem was recently introduced in the context of $f(R)$ theories, by considering a generalized version of the virial theorem [16]. A similar proposal, based upon a possible unification and interaction of dark matter and dark energy, had been put forward before, using similar considerations [17]. Assuming a steady state, the virial theorem can be used to deduce the mean density of astrophysical objects, and therefore the corresponding total mass, such as galaxies and clusters, by observing the velocities of test particles rotating around them. The overall mass of a sample of clusters can also be estimated through corrections in the gravitational potential that

* orfeu.bertolami@fc.up.pt

[†] Also at Instituto de Plasmas e Física Nuclear, Instituto Superior Técnico, Av. Rovisco Pais, 1, 1049-001, Lisboa Portugal.

[‡] pedro.frazao@ist.utl.pt

[§] paramos@ist.edu

emerge in the weak field limit of these theories [18]. Along with these works, there were also conducted the first cluster abundance constraints on a modified gravity model, specifically the modified action $f(R)$ model, which predict deviations in the abundance of massive dark matter halos [19].

Following Ref. [11], it has been argued in several works that both dark energy and dark matter can be effectively described within the framework of a non-minimal coupling between geometry and matter, together with other cosmological and astrophysical implications: these include the perturbed hydrostatic equilibrium of the sun [20], the acceleration of the universe [21], the galaxy rotation curves [10], the reheating scenario after inflation [22], the mimicking of a Cosmological Constant [23] and the change in the gravitational potential [24].

In order to extend this non-minimally coupled model to the study of clusters, one explores here the scenario of the Abell cluster A586. This cluster is a nearby massive strong lensing cluster, with a high X-ray luminosity, related with the mass of the intracluster gas. Its morphology is well suited to the assumption of spherical symmetry, making it an ideal testbed for modifications of gravity at extra-galactic scales.

This work is organized as follows. First, one shortly reviews the formalism leading to the total cluster mass and the field equations that result with the presence of the non-minimal coupling, and sees how to work out the problem of mimicking the dark matter component of a cluster. Then one studies the particular case of the Abell cluster A586 and discusses the coupling function that leads to the dark matter mimicking. In the last sections, the numerical results are presented and discussed.

II. GALAXY CLUSTERS

A. Hydrostatic equilibrium equation

Galaxy clusters are usually considered as closed gravitational systems with spherical symmetry and in hydrostatic equilibrium when virial equilibrium is attained — despite the fact that recent observations reveal that clusters in general have more evolved structures with strong interactions and dynamical activity, particularly in their inner regions [25, 26].

Under these assumptions, the structure equation can be derived from the collisionless Boltzmann equation for an isotropic system [18, 27]

$$\frac{d}{dr} (\rho_g \sigma_r^2) = -\rho_g \frac{d\Phi}{dr} , \quad (1)$$

where Φ is the gravitational potential of the cluster, σ_r the mass-weighted velocity dispersion in the radial direction, and ρ_g the gas mass-density. The pressure profile is related with these quantities through, $P = \sigma_r^2 \rho_g$, and inserting in Eq. (1) leads to $P' = -\rho_g \Phi'$, where the

prime indicates differentiation with respect to the radial coordinate.

For a gas sphere, with temperature profile $T(r)$, the velocity dispersion becomes $\sigma_r^2 \equiv \sum_i < v_i^2 > -v_i^2 = kT/\mu m_p$, where k is the Boltzmann constant, $\mu \approx 0.609$ the mean mass particle, and m_p the proton mass. Introducing this expression into Eq. (1) gives

$$\frac{d}{dr} \left(\frac{kT}{\mu m_p} \rho_g \right) = -\rho_g \frac{d\Phi}{dr} , \quad (2)$$

or, equivalently,

$$-\frac{d\Phi}{dr} = \frac{kT}{\mu m_p r} \left[\frac{d \ln \rho_g}{d \ln r} + \frac{d \ln T}{d \ln r} \right] . \quad (3)$$

Therefore, from the models for the gas density and temperature profiles, the total mass enclosed in a sphere with given radius r can be obtained from the hydrostatic equilibrium equation

$$M(r) = -\frac{kT}{G\mu m_p} r \left[\frac{d \ln \rho_g}{d \ln r} + \frac{d \ln T}{d \ln r} \right] , \quad (4)$$

and is composed by different contributions: gas mass + mass of galaxies + cD-galaxy mass + dark matter. In general, the galaxy part contribution is considered negligible with respect to the other two components such that $M \approx M_g + M_{dm}$.

The equilibrium equation, Eq. (4), which leads to the total mass within a cluster, can be used to derive the amount of dark matter present in a cluster of galaxies, and its spatial distribution, by the mass difference between this and the gas-mass estimates that are provided by X-ray observations.

In the following, one tries to reproduce the total mass profiles for a particular cluster, the Abell cluster A586, where the additional density component emerges not from an exotic form of “dark” matter, but from a change in geometry due to the presence of the non-minimal coupling in the action.

B. Cluster density profiles

Clusters of galaxies present a velocity dispersion with a relative constant value along the radius, which reveals an implicit matter density profile of the form $\rho_M \propto r^{-2}$. The singular isothermal sphere is the simplest model whose density profile, $\rho_M = \sigma_v^2/2\pi G r^2$, leads to a constant and isotropic velocity dispersion σ_v along the clusters profile.

However, numerical simulations to the observational data show that the density profile of clusters are flatter than the isothermal one at small radii and steeper at larger radii. A general form replicating this behaviour is given by the cusped density profile,

$$\rho_M = \rho_0 \left(\frac{r}{r_s} \right)^{-p} \left(1 + \frac{r}{r_s} \right)^{p-q}, \quad (5)$$

where the parameters p and q determine the respective slopes of the power-law density profile in the inner and outer regions, and r_s is the so-called core radius, signaling the steepening of the profile. These parameters usually present values within the ranges $1 \lesssim p \lesssim 1.5$ and $2.5 \lesssim p \lesssim 3$, for models such as the NFW profile, for $p = 1$ and $q = 3$, the Moore profile, for $p = 1.5$ and $q = 3$, and the Rasia profile, for $p = 1$ and $q = 2.5$. In fact, one of the important results of hierarchical CDM models is that the density profile of cold dark matter halos is described by the Navarro-Frenk-White (NFW) model [28].

The more relevant baryonic component is the ICM in the form of hot gas, which emits observable X-ray radiation. In general, the observed surface-brightness profiles of clusters, that reveal the underlying visible matter profile of this intracluster gas, are well described by the so-called β -model of the form $\rho_g = \rho_0 (1 + r^2/r_c^2)^{-3\beta/2}$, where r_c is the core radius, which has a specific value for each cluster [29].

C. Abell Cluster A586

In this cluster, the emission measured profile is described by the following model [30]:

$$\rho_g(r) = \rho_{g0} \left(1 + \frac{r^2}{r_c^2} \right)^{-3\beta/2}. \quad (6)$$

From a least-square fit of the available data, the obtained values for the free parameters are $\beta = 0.518 \pm 0.006$ and $r_c = 67 \pm 2 \text{ } h_{70}^{-1} \text{ kpc}$ [30]. This analytical expression results from a simple modification of the usual β -model. The ICM particle number density profile is given directly by the analytic fit to the projected emission measure profile, Eq. (6), and is easily converted into the gas density.

The deep potential well of the cluster compresses the ICM gas to X-ray emitting temperatures, such that the gas temperature can be inferred from the derived spectrum. For a polytropic temperature model [30],

$$T(r) = T_0 \left(1 + \frac{r^2}{r_c^2} \right)^{-3\beta(\gamma-1)/2}, \quad (7)$$

where r_c and β are the parameters obtained in the fit for the visible mass density, a least-square fit leads to the values $T_0 = 8.99 \pm 0.34 \text{ keV}$ and $\gamma = 1.10 \pm 0.03$ [30]. Naturally, setting $\gamma = 1$ leads to the isothermal temperature profile.

The total mass follows from the hydrostatic equilibrium equation, Eq. (4), using the previous expressions for the visible density and temperature profile

$$M(r) = M_0 \left(\frac{r}{r_c} \right)^3 \left(1 + \frac{r^2}{r_c^2} \right)^{-1 - \frac{3}{2}(\gamma-1)\beta}, \quad (8)$$

with

$$M_0 = \frac{3kT_0\beta\gamma r_c}{G\mu m_p}. \quad (9)$$

One may approximate the dark matter density by

$$\begin{aligned} \rho_{dm}(r) &\approx \frac{M'(r)}{4\pi r^2} = \\ \rho_{dm0} &\left(1 + \epsilon \frac{r^2}{r_c^2} \right) \left(1 + \frac{r^2}{r_c^2} \right)^{-2 - \frac{3}{2}(\gamma-1)\beta}. \end{aligned} \quad (10)$$

where

$$\rho_{dm0} = \frac{3kT_0\beta\gamma}{4\pi G\mu m_p r_c^2} = \frac{M_0}{4\pi r_c^3}, \quad (11)$$

and one defines $\epsilon \equiv [1 + 3(1 - \gamma)]\beta$, for convenience.

Finally, one introduces the virial radius r_V , which signals the distance where the density of the cluster approaches a multiple α of the critical density of the universe $\rho_c = 3H_0^2/8\pi G$, where H_0 is the Hubble parameter in the present time. Thus, from $\rho_{dm}(r_V) = \alpha\rho_c$, one may estimate the virial radius from the relation Eq. (10),

$$\frac{r_V}{r_c} \approx \left(\frac{\rho_{dm0}}{\rho_c} \frac{\epsilon}{\alpha} \right)^{\frac{1}{2-\epsilon+\beta}}, \quad (12)$$

which, for $\rho_{dm} \approx 200\rho_c$, with $\alpha = 200$, leads to a virial radius of $r_V \approx 1.497 \text{ Mpc}$.

III. THE NON-MINIMAL COUPLING

A. Field equations

Recently, it was considered a generalization of the $f(R)$ modified theories of gravity that further extends the presence of curvature invariant terms in the Einstein-Hilbert action by coupling non-minimally the scalar curvature with matter [11]. The action is obtained by adding an additional $f(R)$ term, dependent on the scalar curvature R and coupled with the matter Lagrangian \mathcal{L}_m , to the usual metric theories of gravity, such that [11]

$$S = \int \left[\frac{1}{2} f_1(R) + [1 + f_2(R)] \mathcal{L}_m \right] \sqrt{-g} d^4x, \quad (13)$$

where $f_i(R)$ (with $i = 1, 2$) are arbitrary functions of the scalar curvature and g is the metric determinant. Setting

$f_2(R) = 0$ one obtains the usual $f(R)$ theories of gravity, and GR is recovered if one takes the linear function $f_1(R) = 2\kappa R$, where $\kappa = c^4/16\pi G$.

Variation with respect to the metric, $g_{\mu\nu}$, leads to the field equations,

$$(F_1 + 2F_2\mathcal{L}_m) R_{\mu\nu} - \frac{1}{2}f_1 g_{\mu\nu} = (\Box_{\mu\nu} - g_{\mu\nu}\Box)(F_1 + 2F_2\mathcal{L}_m) + (1 + f_2)T_{\mu\nu} \quad , \quad (14)$$

where $T_{\mu\nu}$ is the energy-momentum tensor. The respective trace equation is given by

$$(F_1 + 2F_2\mathcal{L}_m) R - 2f_1 = -3\Box(F_1 + 2F_2\mathcal{L}_m) + (1 + f_2)T \quad . \quad (15)$$

B. Non-conservation of the energy momentum tensor

From the covariant derivative of the field equations, Eqs. (14), along with the Bianchi identities, $\nabla^\mu G_{\mu\nu} = 0$, one encounters the covariant non-conservation of the energy-momentum tensor [11]

$$\nabla^\mu T_{\mu\nu} = (g_{\mu\nu}\mathcal{L}_m - T_{\mu\nu})\nabla^\mu \log(1 + f_2) \quad , \quad (16)$$

which can be regarded as an energy-momentum exchange between matter and geometry. The usual covariant conservation for the energy-momentum tensor is naturally obtained when the non-minimal coupling vanishes, $f_2(R) = 0$.

This non-conservation implies that a massive particle in the absence of forces will not describe a geodesic curve. Strong variations on the extra term in the last equation can imply a violation of the Equivalence Principle, leading to a possible way of testing and setting bounds on the coupling functions, $f_2(R)$. Contrary to the usual Jordan-Brans-Dicke theories, it is impossible to perform a conformal transformation to the Einstein frame such that the coupling disappears and the covariant conservation of the energy-momentum tensor is recovered for all matter forms [32].

Indeed (following Ref. [32]), using the conformal transformation

$$g_{\mu\nu} \rightarrow \tilde{g}_{\mu\nu} = f_2 g_{\mu\nu} \quad , \quad (17)$$

one obtains the covariant conservation law

$$\tilde{\nabla}_\mu \tilde{T}^{\mu\nu} = 0 \quad , \quad (18)$$

only if $\tilde{T}^{\mu\nu} = f_2^{-2} T^{\mu\nu}$ and $2\mathcal{L} = T$. From the energy-momentum tensor of a perfect fluid, $T_{\mu\nu} = (\rho + p)u_\mu u_\nu + pg_{\mu\nu}$, where ρ is the energy density, p the pressure and

U_μ the four-velocity (with $U_\mu U^\mu = -1$), the respective trace is, $T = 3p - \rho$, such that one may write,

$$2\mathcal{L} = 3p - \rho \quad \rightarrow \quad p = (2\mathcal{L} + \rho)/3 \quad . \quad (19)$$

However, one obtains different equations of state depending on the chosen Lagrangian density \mathcal{L} . For instance, if $\mathcal{L} = -\rho$ [31], one has the state equation $p = -\rho/3$, a perfect fluid with negative pressure, not a cosmological constant with $p_\Lambda = -\rho_\Lambda$; and for $\mathcal{L} = p$, then $p = \rho$, which is the equation of state for ultra-stiff matter. Therefore, this non-conservation is in fact a fundamental property of the model, Eq. (13), meaning that even under a suitable conformal transformation the energy momentum tensor is not conserved for all different types of matter.

Assuming that matter is described by a perfect fluid, the non-conservation, Eq. (16), results in an extra force of the form

$$f^\mu = \frac{1}{\rho + p} \left[(\mathcal{L}_m + p) \nabla_\nu \log(1 + f_2) + \nabla_\nu p \right] h^{\mu\nu} \quad (20)$$

which has units of an acceleration, and where the projection operator is given by $h_{\mu\nu} = g_{\mu\nu} - U_\mu U_\nu$, such that the extra force is orthogonal to the four-velocity, $h_{\mu\nu} U^\mu = 0$.

C. Mimicking the dark matter component

In order to test the effect of the non-minimal coupling, one focuses on possible deviations from GR due to the presence of the coupling by considering the linear function $f_1(R) = 2\kappa R$; following Ref. [10], one adopts a power-law non-minimal coupling

$$f_2(R) = \left(\frac{R}{R_n} \right)^n \quad . \quad (21)$$

where R_n is a characteristic curvature.

Considering a pressureless perfect fluid, $T_{\mu\nu} = \rho U_\mu U_\nu$, and the respective trace equation, $T = -\rho$, along with the Lagrangian density, $\mathcal{L}_m = -\rho$ (a choice discussed in depth in Ref. [31]), the field Eqs. (14) become

$$\begin{aligned} & \left[1 - \frac{n}{\kappa} \left(\frac{R}{R_n} \right)^n \frac{\rho}{R} \right] R_{\mu\nu} - \frac{1}{2} R g_{\mu\nu} = \\ & = \frac{n}{\kappa} (g_{\mu\nu} \Box - \Box_{\mu\nu}) \left[\left(\frac{R}{R_n} \right)^n \frac{\rho}{R} \right] \\ & \quad + \frac{1}{2\kappa} \left[1 + \left(\frac{R}{R_n} \right)^n \right] \rho U_\mu U_\nu \quad , \end{aligned} \quad (22)$$

and the respective trace, Eq. (15), reads

$$R = \frac{1}{2\kappa} \left[1 + (1 - 2n) \left(\frac{R}{R_n} \right)^n \right] \rho - \frac{3n}{\kappa} \square \left[\left(\frac{R}{R_n} \right)^n \frac{\rho}{R} \right] . \quad (23)$$

If one considers a strong coupling $(R/R_n)^n \gg 1$, the above has an implicit, “static”, solution, given by the vanishing of the second term in the *r.h.s.*,

$$\frac{R}{R_n} = \frac{\rho_{dm}}{\rho_n} \approx \left[(1 - 2n) \frac{\rho}{\rho_n} \right]^{1/(1-n)} , \quad (24)$$

where one introduces the characteristic density, $\rho_n \equiv 2\kappa R_n$.

Considering the tensorial character of the field Eqs. (14), one obtains the following relation between the energy density and pressure of the mimicked dark matter component [10],

$$\rho_{dm} = \frac{1 - n}{1 - 4n} 2\kappa R , \quad (25)$$

$$p_{dm} = \frac{n}{1 - 4n} 2\kappa R . \quad (26)$$

From Eq. (24), one has a relation between the visible and dark matter density profiles,

$$\frac{\rho_{dm}}{\rho_n} = \frac{1 - n}{1 - 4n} \left[(1 - 2n) \frac{\rho}{\rho_n} \right]^{1/(1-n)} . \quad (27)$$

The above clearly shows that one may obtain a “dark” component from the visible matter density profile, with a change of slope given by the scaling exponent $1/(1 - n)$.

For convenience, Eq (23), can be rewritten in a dimensionless form, by defining the rescaled quantities [10],

$$y \equiv \frac{r_n}{r} , \quad (28)$$

$$\theta \equiv \left(\frac{\rho}{\rho_n} \right)^{1/(1-n')} , \quad (29)$$

$$\varrho \equiv \frac{2\kappa R}{\rho_n \theta} = \frac{1}{\theta} \frac{R}{R_n} , \quad (30)$$

where one defines the length scale, $r_n = 1/\sqrt{R_n}$. The resulting dimensionless form of the trace Eq. (23) is

$$\varrho = \theta^{-n} + (1 - 2n)\varrho^n - \frac{6n}{\theta} \bar{\square} (\varrho^{n-1}) , \quad (31)$$

where $\bar{\square} = y^4 d^2/d^2 y$. The equivalent to the “static” solution, Eq. (24), is thus, $\varrho = (1 - 2n)^{1/(1-n)}$, as may be easily checked.

Concluding, one uses the visible matter density profile ρ , which in a cluster is approximately equal to the ICM gas density, $\rho \approx \rho_g$, in Eq. (29), to solve the differential equation Eq. (31), leading to a dark matter component that can account for the large mass difference in the cluster total density profile, as will be discussed in section IV B.

D. Non-geodesic motion

Before dwelling into the analytical and numerical details of the scenario under scrutiny, one must first consider a possible issue: the presence of an extra-force, as given by Eq. (20). Considering a pressureless perfect fluid along with the Lagrangian, $\mathcal{L}_m = -\rho$, the same equation reduces to

$$f^\mu = -\nabla_\nu \log(1 + f_2) h^{\mu\nu} . \quad (32)$$

For spherical symmetry, the radial component is

$$f^r = -\partial_r \log(1 + f_2) = -\frac{F_2(R)}{1 + f_2(R)} R' , \quad (33)$$

where the prime denotes derivative with respect to the radial coordinate. Considering a power-law coupling of the form of Eq. (21), one has

$$f^r = -n \frac{(R/R_n)^n}{1 + (R/R_n)^n} \frac{R'}{R} . \quad (34)$$

If the curvature R decreases along the radius, a negative exponent n will produce an inward binding force, and a positive one an outward force, which could break the stability of an orbit.

As already seen in a previous work [10], different solutions for the differential equation, Eq. (31), lead to different behaviours of this extra-force, depending on the relevance of the coupling function. If it dominates, $(R/R_n)^n \gg 1$, then the force becomes

$$f_r \approx -n \frac{R'}{R} . \quad (35)$$

On the contrary, a perturbative regime leads to a suppression of the expression above by a factor $(R/R_n)^n \ll 1$,

$$f_r \approx -n \left(\frac{R}{R_n} \right)^n \frac{R'}{R} . \quad (36)$$

The “static” solution given by Eq. (24) is derived from the dominant condition $f_2(R) \gg 1$; taking only the outer slope behaviour of cusped density profiles for the dark matter component, $\rho_{dm} \propto r^{-m}$, and a positive exponent n (as will be used in the following section), one concludes that the extra force has an outward direction,

$$f_r \approx -n \frac{R'}{R} \sim -n \frac{\rho'_{dm}}{\rho_{dm}} = \frac{nm}{r} . \quad (37)$$

For n and m of order unity, one obtains a force much greater than the Newtonian counterpart, $f_N =$

$GM(r)/r^2$, thus destabilizing the orbital motion of test particles. In the inner region, $r \ll r_c$, one has an approximately constant dark matter density, $\rho_{dm} \approx \rho_{dm0}$, yielding a negligible extra force.

However, it was shown in Ref. [10] that the most general solution of the differential, Eq. (31), is not the “static” solution, $\varrho = (1 - 2n)^{1/(1-n)}$, because the gradient terms on the *r.h.s.* of this equation are dominant: the system instead follows a “dynamical” solution, ϱ , that exhibits very small oscillations around a constant value. It was shown that, although the above analytical treatment remains valid, this implicates that the non-minimal coupling is actually perturbative, *i.e.* $f_2 = (R/R_n)^n \ll 1$.

For a fixed R_n , it is then clear that $f_2(R)$ increases for lower values of a positive exponent n ; thus, one expects that there is a lower bound on n , such that the condition $f^r < f_N$ fails due to the insufficient suppression of the extra force f^r .

In order to assess the value of this lower bound, one first uses Eqs. (8) and (10) to write the following approximations, valid in the large radius region $r \gg r_c$:

$$M(r) \sim M_0 \left(\frac{r}{r_c} \right)^{1+\epsilon-\beta}, \quad (38)$$

$$\rho_{dm} \sim \rho_{dm0} \epsilon \left(\frac{r}{r_c} \right)^{-2+\epsilon-\beta}.$$

Using the above, one may write

$$f_r \approx -n \left(\frac{R}{R_n} \right)^n \frac{R'}{R} \sim -n \left(\frac{\rho_{dm}}{\rho_n} \right)^n \frac{\rho'_{dm}}{\rho_{dm}} \sim \quad (39)$$

$$(2 - \epsilon + \beta) \frac{n}{r_c} \left(\frac{\rho_{dm0}}{\rho_n} \epsilon \right)^n \left(\frac{r}{r_c} \right)^{(-2+\epsilon-\beta)n-1},$$

so that, writing $\rho_{dm0} = 2\kappa/r_0^2$, the perturbative condition $f^r \ll f_N = GM(r)/r^2$ reads

$$\sqrt{2n(2 - \epsilon + \beta)} \frac{r_0}{r_c} \left(\sqrt{\epsilon} \frac{r_n}{r_0} \right)^n \left(\frac{r}{r_c} \right)^{(\epsilon-\beta)\frac{n-1}{2}-n} \ll 1. \quad (40)$$

One now assumes that $-2n + (\epsilon - \beta)(n - 1) > 0$ (as is the case with the Abell cluster A586, discussed in the following section). Thus, the relevance of the extra force decreases with the distance from the cluster’s center, and one may saturate the *l.h.s.* of the above equation by setting $r \sim r_c$, yielding

$$b(r_n, n) \equiv \sqrt{2n(2 - \epsilon + \beta)} \left(\sqrt{\epsilon} \frac{r_n}{r_0} \right)^n \frac{r_0}{r_c} \ll 1. \quad (41)$$

Finally, notice that, for a positive exponent n , the perturbative condition $f_2 \ll 1$ translates into

$$\left(\frac{R}{R_n} \right)^n \ll 1 \rightarrow \rho_{dm0} \ll 2\kappa R_n \rightarrow r_0 \gg r_n. \quad (42)$$

Thus, a lower exponent n will increase the *l.h.s.*, as expected. The following section will discuss this lower bound on n in the case of the Abell cluster A586.

IV. THE ABELL CLUSTER A586 CASE

A. Density Profiles

After considering the possibilities offered by the non-minimally coupled model in the previous sections, one now implements the mimicking of the dark matter component of the cluster in consideration.

Recalling Eqs. (6) and (38), one writes the approximations valid in the large radius regime $r \gg r_c$,

$$\rho_g \sim \left(\frac{r}{r_c} \right)^{-3\beta}, \quad \rho_{dm} \sim \left(\frac{r}{r_c} \right)^{-2-3(\gamma-1)\beta}. \quad (43)$$

Therefore, from the scaling given in Eq. (27), one obtains the relation $\rho_{dm} \sim \rho^{1/1-n}$, allowing for an estimation of the expected value of the n exponent:

$$n = \frac{2 + 3(\gamma - 2)\beta}{2 + 3(\gamma - 1)\beta} \approx 0.279, \quad (44)$$

using $\beta = 0.518$ and $\gamma = 1.10$ [30]; and, for the isothermal case with $\gamma = 1$,

$$n = 1 - \frac{3\beta}{2}(2 - \gamma) \approx 0.223. \quad (45)$$

Hence, the results coming from the presence of the non-minimal coupling should be similar of whether one is considering an isothermal or a polytropic temperature profile.

B. Numerical results

In order to mimic the dark matter component of this cluster, one numerically solves the differential Eq. (31), for an assumed gas density profile, as given by Eq. (6), and varies the parameters R_n and n in order to obtain a best fit between the derived mimicked dark matter density $\rho_{total} - \rho_{gas}$ and the observed curve. The considered range for the numerical integration lies between $r_i = 10r_s$, the Schwarzschild radius of the Cluster, and a sufficiently large radius, above the observed size of the cluster.

The results of the numerical simulations are shown in Fig. (1) and the resulting integrated mass radial profile, $M(r) = \int_0^r \rho(r') dr'$, in Fig. (2), for the values of $n = 0.23, 0.33, 0.43, 0.53$, and 0.63 , with a best fit attained for $n = 0.43$; $r_n = 10^{-2}$ pc is kept constant, as its value does not change the mimicked dark matter density

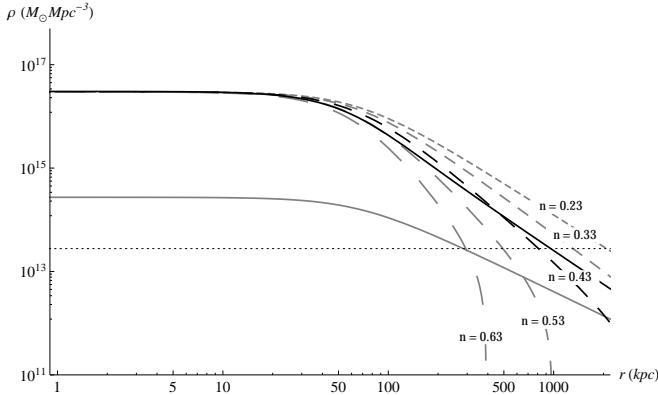


FIG. 1. Mass density profiles for the visible matter component (gray), the total density profile from the hydrostatic equilibrium equation (dark), and the mimicked density profiles (dashed) for different values of n , where the dashing length increases with n . The best-fit obtained is for $n = 0.43$ (dark dashed) and the horizontal dotted line is for $\rho = 200\rho_c$.

n	$r_V(\text{Mpc})$	$M_V(M_\odot)$	$ 1 - M_{\text{mim}}/M (\%)$
0.23	2.089	3.08×10^{15}	308.81
0.33	1.309	9.99×10^{14}	124.03
0.43	0.810	3.42×10^{14}	6.94
0.53	0.493	1.28×10^{14}	56.05
0.63	0.294	5.13×10^{13}	83.77

TABLE I. Virial radius and respective mass for $\rho_{dm} \approx 200\rho_c$. Mass differences for different values of the n evaluated at $r = 1.165$ Mpc.

profile (as discussed below). This value for the exponent n is determined by the minimization of the relative difference between the obtained mimicked total mass and that expected from the hydrostatic estimative, Eqs. (4) and (8), with values shown in Table (I).

As one can see, these results show that, in the outer regions of the cluster, the density decreases with the value of the n along with a decrease in the total mass for the cluster. The best fit $n = 0.43$, is the one that yields a mimicked profile which minimizes the mass difference to only 6.94% at $r_V = 1.165$ Mpc, the virial radius for the density profile derived from Eqs. (6) and (8). In fact, in Fig. (2), one can see that the values in the range, $n < 0.43$, lead to a dynamical mass larger than the upper limit set by the model, $M = 4.25 \times 10^{14} M_\odot$.

Notice that this best fit $n = 0.43$ deviates from the expected value $n = 0.279$, computed in Eq. (44). As the curves for $n = 0.33$ and $n = 0.23$ show, this stems from the fact that the mimicked dark matter density arising from the expected value is unable to follow the observed profile. Indeed, while $n = 0.279$ yields the same slope as the observed total mass density, it leads to a right-shifted curve, giving rise to a much higher total mass for the cluster.

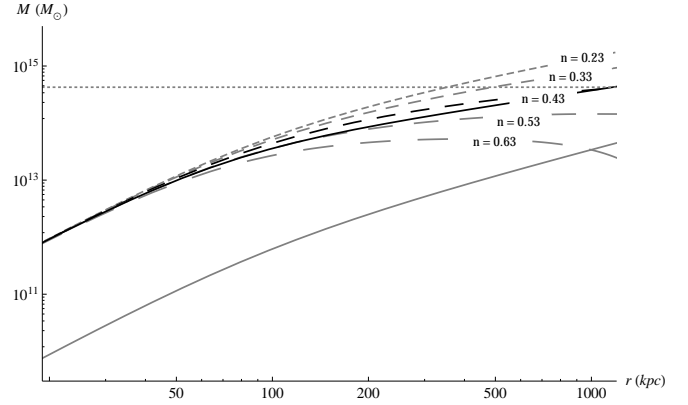


FIG. 2. Mass radial profile, resulting from the integration of the mass density profile. The dotted line is for the dynamical mass of $M = 4.25 \times 10^{14} M_\odot$ (polytropic case) [30].

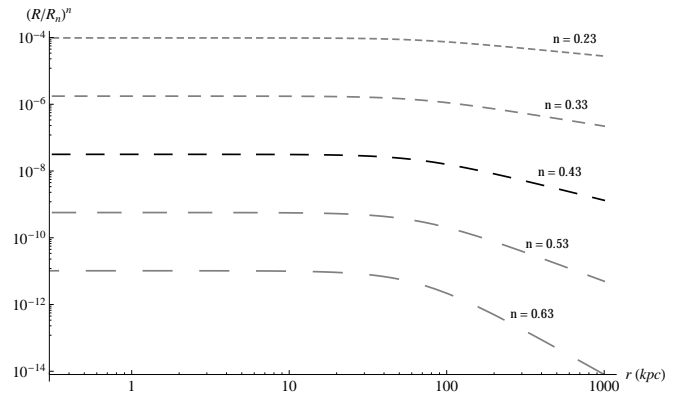


FIG. 3. Resulting power-law couplings, $f_2(R) = (R/R_n)^n$, after the integration of the differential equation, Eq. (31), for different values of n .

Numerically, one finds that the mimicked dark matter profile is almost independent of the characteristic length scale r_n , provided one sets the bound $r_n \lesssim 1$ Mpc. This independence is easily explained: a different r_n induces a change in the boundary conditions of Eq. (31), which translates into a change of the dimensionless solution ϱ (not shown); however, this is counteracted by the presence of r_n in the relation between the latter and the mimicked dark matter density, Eq. (29).

Fig. (4) shows that values above $r_n \sim 1$ Mpc lead to a mimicked dark matter density that strongly deviates from the observed profile, with a sharp rise (and a subsequent fall into the expected outer slope). The onset of this rise decreases with higher values of r_n — *i.e.*, lower values of R_n .

Despite the complexity of the differential Eq. (31), the existence of an upper bound for this independence seems to be due to the fact that, since the exponent n is positive in the considered range, a lower $R_n = 1/r_n^2$ translates into an increased value of $f_2(R)$: as r_n approaches $r_0 \approx 12.8$ Mpc from below, one eventually gets $(R/R_n)^n \sim 1$ (in the inner, higher curvature region), in

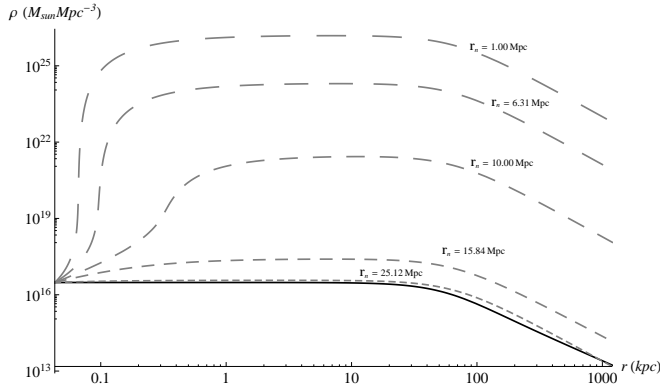


FIG. 4. Plot of different dark matter mimicked density profiles for different values of the characteristic length scale, $r_n = 1.00, 6.31, 10.00, 15.84, 25.12$ Mpc, where the dashed increases with the value of r_n , compared with the observed dark matter component (black). These values are obtained for the best fit value $n = 0.43$.

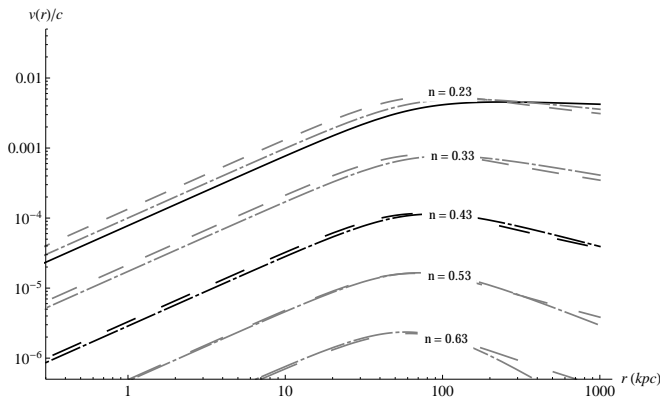


FIG. 5. Additional radial velocity resulting from the non-geodesic motion due to the dark matter component (dashed) and to the mimicked dark matter (dot-dashed) for different values of n , the same of Fig. (1), and also for the total density profile (black).

contradiction with the assumption of a perturbative non-minimal coupling.

1. Non-geodesic motion

In Fig. (5) one presents the plot of the additional radial velocity $\Delta v = \sqrt{r f^r}$ arising from non-geodesic motion as a function of distance to the cluster's center, for the considered range of values for n . Notice that, despite the fact that the observable quantity is the velocity dispersion σ , estimated from the velocities of individual clusters, these curves enable one to see the relevance of the extra forces that appear due to the presence of the non-minimal coupling.

Since the scalar curvature (*i.e.* the total density) is de-

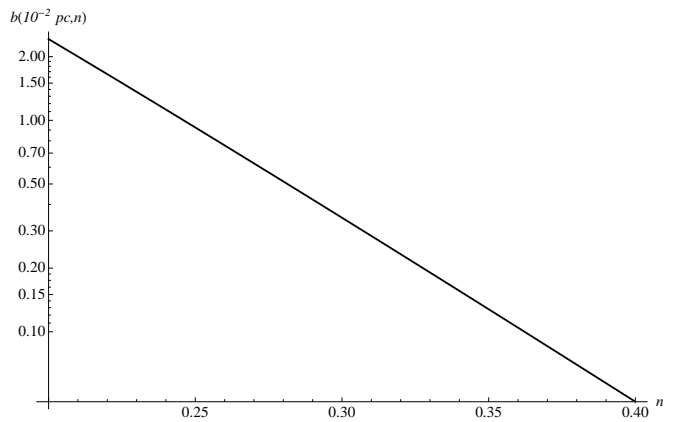


FIG. 6. Variation of $b(r_n = 10^{-2} \text{ pc}, n)$.

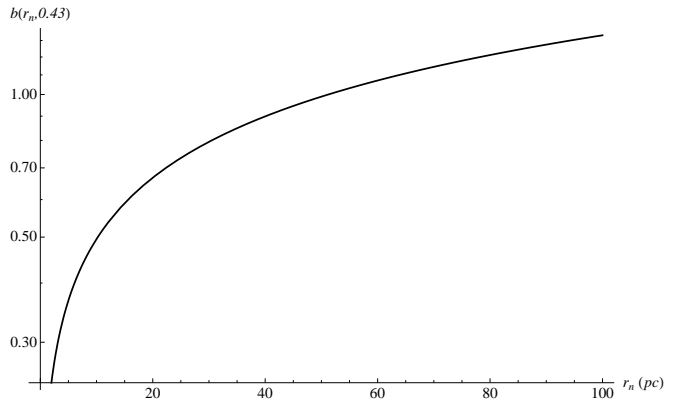


FIG. 7. Variation of $b(r_n, n = 0.43)$.

creasing, one concludes that the related force counteracts the gravitational attraction, as discussed in section III B. Thus, stability requires that this additional velocity be much smaller than the Newtonian radial velocity profile: this is attained for higher values of n . In particular, one concludes that a power-law coupling with $n = 0.43$ can effectively mimic the dark matter component of the Abell cluster A586, with a negligible effect on the velocity profile $v(r)$.

As already discussed in section III D, one expects a decrease of the effect of the extra force for increasing exponent n (for fixed r_n). Indeed, as Fig. 3 depicts, the considered range always leads to a perturbative $f_2(R)$. However, as Fig. 6 shows, values of $n \lesssim 0.23$ do not enable a sufficiently strong suppression of the extra force: although the additional (outward) radial velocity is indeed smaller than c , it may still be above the Newtonian counterpart.

Using Eq. (11) and the relevant values obtained from Ref. [30], one has $\epsilon = 0.3626$ and $\rho_{dm0} \approx 10^{16} M_{\odot}/\text{Mpc}^3 \rightarrow r_0 \approx 12.8$ Mpc. Inserting this into Eq. (41), together with $r_c = 67$ kpc and $r_n = 10^{-2}$ pc, one finds that the extra force is smaller than the Newtonian force when

$$b(10^{-2} \text{ pc}, n) < 1 \rightarrow n > 0.246 \quad , \quad (46)$$

which should be compared with the aforementioned lower bound $n > 0.23$, obtained from Fig. 5.

The lack of sensitivity of the mimicked dark matter density profile on the value of r_n may be used to establish a more stringent upper bound on this parameter. To do so, one fixes the best fit value $n = 0.43$ and searches for the value of r_n that fulfills the above condition:

$$b(r_n, 0.43) < 1 \rightarrow r_n < 51 \text{ pc} \quad , \quad (47)$$

Variation of $b(r_n = 10^{-2} \text{ pc}, n)$ and $b(r_n, n = 0.43)$ are shown in Figs. 6 and 7, respectively.

C. Relevance in other contexts

The non-minimal coupling here considered may be regarded as an approximation to a more evolved form for $f_2(R)$, which would encompass couplings considered in previous studies, which perhaps hints at a Laurent series,

$$f_2(R) = \sum_{n=-\infty}^{\infty} \left(\frac{R}{R_n} \right)^n \quad . \quad (48)$$

Each term would be valid in a particular regime: early *vs.* late time, central *vs.* long range, galactic *vs.* cluster size, *etc.* In particular, this series should also include the aforementioned $n = -1$ and $n = -1/3$ terms, relevant to mimic dark matter at galactic level, as well as a linear coupling R/R_1 considered in the context of preheating and inflationary dynamics; the corresponding parameters are

$$\begin{aligned} r_{-1} &\equiv (R_{-1})^{-1/2} = 21.5 \text{ Gpc} \quad , \quad (49) \\ r_{-1/3} &\equiv (R_{-1/3})^{-1/2} = 1.69 \times 10^6 \text{ Gpc} \quad , \\ r_1 &\equiv R_1^{-1/2} = 4.8\sqrt{\xi} \times 10^{-29} \text{ m} \quad , \end{aligned}$$

with $10 < \xi < 10^4$ [22].

Since the coupling terms relevant at galactic scales have negative exponents, it is trivial to conclude that their effect is negligible during inflation, when the curvature is much higher. Conversely, the effect of the terms involved in preheating and inflation are irrelevant at astrophysical or cosmological scales at present.

Similarly, the cosmological effect of the best fit coupling with $n = 0.43$ may be disregarded, as it is of the order of

$$\left(\frac{R_{\text{cosmo}}}{R_n} \right)^n \sim \left(\frac{r_n}{r_H} \right)^{2n} < 10^{-3} \quad . \quad (50)$$

Thus, one is left with the possible conflict between astrophysical relevant terms. If one considers three power-law couplings with $n = -1$, $-1/3$ and 0.43 , the resulting dark matter profile will not be a sum of the individual contributions, due to the non-linearity of Eq. (23). Even if one disregards the resulting interaction between terms (a reasonable approximation, as shown in Ref. [10]), the exponents simply yield the slope of each derived dark matter contribution, not their relative values. Indeed, when numerically integrating Eq. (31), one imposes boundary conditions on the overall dark matter density (*i.e.* the dimensionless function ϱ) — the relative contributions of each dark matter component are then determined dynamically.

Given the scaling relation Eq. (24), a larger $n < 1$ implies a steeper dark matter component $\rho_{dm(n)} \sim \rho^{1/(1-n)}$. Resorting to the $\rho \sim r^{-4}$ outer Hernquist profile for the matter distribution of galaxies, one finds

$$\begin{aligned} \rho_{dm(-1)} &\sim r^{-2} \quad , \quad \rho_{dm(-1/3)} \sim r^{-3} \quad , \quad (51) \\ \rho_{dm(0.43)} &\sim r^{-7} \quad . \end{aligned}$$

Thus, the $n = 0.43$ merely gives rise to a quickly decaying component: the $n = -1$ and $n = -1/3$ contributions dominate at large distances, even if the former dominates at short ones. Conversely, the $\rho \sim r^{-3\beta}$ behaviour of the cluster mass density translates into

$$\begin{aligned} \rho_{dm(-1)} &\sim r^{-0.8} \quad , \quad \rho_{dm(-1/3)} \sim r^{-1.2} \quad , \quad (52) \\ \rho_{dm(0.43)} &\sim r^{-2.7} \quad . \end{aligned}$$

In order for the contribution from the $n = -1$ and $-1/3$ to be neglected, it suffices that they are subdominant at short distances. One does not pursue an explicit computation of the effect of these three power-law terms here, given that the main scope was to describe the A586 cluster. Nevertheless, it is not difficult to see that the difference between the typical galactic and cluster scales do allow for a consistent disentangling of the effects of these two sets of terms.

V. CONCLUSIONS AND OUTLOOK

In this work, the possibility of mimicking the dark matter component of a galaxy cluster in the context of a model, Eq. (13), where the scalar curvature is non-minimally coupled with matter is discussed. For that, the cluster A586 has been examined, since it is relaxed and quality data for most of its relevant dynamical parameters is available.

For $f_1(R) = R$, the best fit obtained with a power-law coupling $f_2(R) = (R/R_n)^n$ is for $n = 0.43$, with a strong constraint on the typical length scale $r_n \equiv 1/\sqrt{R_n} < 51 \text{ pc}$ arising from the requirement that the induced extra-force is smaller than the Newtonian one.

A weaker constraint $r_n \lesssim r_0 = 12.8$ Mpc arises from the behaviour of the numerical integration of Eq. (31).

The obtained fit does not correspond to the analytical value for n computed from the scaling relation between dark and visible matter, as the latter would give rise to a mimicked dark matter density that does not follow the observational curve (albeit it falls with the same slope). Instead, a shift from this analytical value is enforced, whereas the mimicked density is slightly steeper than the observed profile, but with a negligible difference in total mass.

Furthermore, the exponent n is high enough so that the non-minimal coupling is perturbative, with $f_2(R) \sim 10^{-8}$ suppressing the destabilizing effect of the outward extra-force arising from the non-conservation of the energy-momentum tensor, as previously found in the context of galaxy rotation curves (where two negative exponents $n = -1$ and $n = -1/3$ were shown to correspond to the

best fit for the rotation curves) [10].

Studies addressing different scenarios have resorted to power-law couplings with different exponents than the best fit value $n = 0.43$ here reported — which may be regarded as another term in a putative series expansion of a more general non-minimal coupling. By the same token, yet unprobed terms of this series may be charted through the study of other phenomena and environments, where distinct curvatures and densities are at play.

This first attempt at modelling the dark component of clusters shows that a consistent approach may be obtained by considering a suitable perturbative non-minimal coupling. In a subsequent work, this method will be extended to more dynamical clusters, using the available profiles for the visible matter density and temperature obtained from modifications of the usual β -model, Eq. (6), and the polytropic temperature profile, Eq. (7), (*cf.* Ref. [33]).

-
- [1] D. N. Spergel *et al.* [WMAP Collaboration], *Ap. J. Supp.* **170**, 377 (2007) [arXiv:astro-ph/0603449]; G. Hinshaw *et al.*, *Ap. J. Supp.* **180**, 225 (2009) [arXiv:0803.0732]; E. Komatsu *et al.*, *Ap. J. Supp.* **180**, 330 (2009) [arXiv:0708.2750]; *Ap. J. Supp.* **192**, 18 (2011) [arXiv:1001.4538].
 - [2] M. Tegmark *et al.* [SDSS Collaboration], *Phys. Rev. D* **74**, 123507 (2006) [arXiv:astro-ph/0608632]; M. Sako *et al.*, *Ap. J. Supp.* **135**, 348 (2008) [arXiv:0708.2750].
 - [3] G. Bertone, D. Hooper and J. Silk, *Physics Reports* **405**, 279 (2005) [arXiv:hep-ph/0404175].
 - [4] E. J. Copeland, M. Sami and S. Tsujikawa, *Int. J. Mod. Phys. D* **15**, 1753 (2006) [arXiv:hep-th/0603057].
 - [5] T. P. Sotiriou and V. Faraoni, *Rev. Mod. Phys.* **82**, 451 (2010) [arXiv:0805.1726].
 - [6] S. Capozziello and M. Laurentis, to appear in *Physics Reports* (2011) [arXiv:1108.6266].
 - [7] S. Capozziello and M. Francaviglia, *Gen. Relativity and Gravitation* **40**, 357 (2008) [arXiv:astro-ph/0706.1146].
 - [8] S. Capozziello, V. F. Cardone and A. Troisi, *JCAP* **08**, 001 (2006) [arXiv:astro-ph/0602349].
 - [9] S. Capozziello, V. F. Cardone and A. Troisi, *Mon. Not. R. Ast. Soc.* **375**, 1423 (2007) [arXiv:astro-ph/0603522].
 - [10] O. Bertolami and J. Páramos, *JCAP* **03**, 009 (2010) [arXiv:0906.4757].
 - [11] O. Bertolami, C. G. Böhmert, T. Harko and F. S. N. Lobo, *Phys. Rev. D* **75**, 104016 (2007) [arXiv:0704.1733].
 - [12] G. M. Voit, *Rev. Mod. Phys.* **77**, 207 (2005) [arXiv:astro-ph/0410173].
 - [13] M. Milgrom, *Ap. J.* **270**, 365 (1983).
 - [14] O. Bertolami and J. Páramos, (2006) [arXiv:gr-qc/0611025].
 - [15] R. H. Sanders, *Mon. Not. R. Ast. Soc.* **342**, 901 (2003) [arXiv:astro-ph/0212293].
 - [16] Francisco S. N. Lobo, (2008) [arXiv:0807.1640].
 - [17] O. Bertolami, F. Gil Pedro and M. Le Delliou, *Phys. Lett. B* **654**, 165 (2007) [arXiv:astro-ph/0703462]; *Gen. Relativity and Gravitation* **41**, 2839 (2009) [arXiv:0705.3118]; (2011) [arXiv:1105.3033].
 - [18] S. Capozziello, E. De Filippis and V. Salzano, *Mon. Not. R. Ast. Soc.* **394**, 947 (2009) [arXiv:0809.1882].
 - [19] F. Schmidt, A. Vikhlinin and W. Hu, *Phys. Rev. D* **80**, 083505 (2009) [arXiv:0908.2457].
 - [20] O. Bertolami and J. Páramos, *Phys. Rev. D* **77**, 084018 (2008) [arXiv:0709.3988].
 - [21] O. Bertolami, P. Frazão and J. Páramos, *Phys. Rev. D* **81**, 104046 (2010) [arXiv:1003.0850].
 - [22] O. Bertolami, P. Frazão and J. Páramos, *Phys. Rev. D* **83**, 044010 (2011) [arXiv:1010.2698].
 - [23] O. Bertolami and J. Páramos, *Phys. Rev. D* **84**, 064022 (2011) [arXiv:1107.0225].
 - [24] O. Bertolami and A. Martins, (2011) [arXiv:1110.2379].
 - [25] D. Chakrabarty, E. De Filippis and H. Russell, *Astronomy & Astrophysics* **487**, 1988 (2008) [arXiv:0806.0009].
 - [26] M. Sereno, E. De Filippis, G. Longo, M. W. Bautz, *Ap. J.* **645**, 170 (2006) [arXiv:astro-ph/0806.0009].
 - [27] S. Capozziello, M. De Laurentis, S. D. Odintsov and A. Stabile, *Phys. Rev. D* **83**, 064004 (2011) [arXiv:1101.0219].
 - [28] J. F. Navarro, C. S. Frenk and S. D. M. White, *Ap. J.* **462**, 563 (1996) [arXiv:astro-ph/9508025].
 - [29] A. Cavaliere and R. Fusco-Femiano, *Astronomy & Astrophysics* **49**, 137 (1976); **70**, 677 (1978).
 - [30] E. S. Cypriano, G. B. Lima Neto, L. Sodré, J. P. Kneib and L. E. Campusano, *Ap. J.* **630**, 38 (2005) [arXiv:astro-ph/0504036].
 - [31] O. Bertolami, F. S. N. Lobo and J. Páramos, *Phys. Rev. D* **78**, 064036 (2008) [arXiv:0806.4434].
 - [32] T. P. Sotiriou and V. Faraoni, *Class. Quantum Gravity* **25**, 205002 (2008). [arXiv:0805.1249].
 - [33] A. Vikhlinin, A. Kravtsov, W. Forman, C. Jones, M. Markevitch, S. S. Murray and L. V. Speybroeck, *Ap. J.* **640**, 691 (2006) [arXiv:astro-ph/0507092].